**Geomechanics and Engineering**, *Vol. 26, No. 2 (2021) 191-204*
https://doi.org/10.12989/gae.2021.26.2.191


# Deformation behavior analysis of tunnels opened in various rock mass grades conditions in China

Jian Zhou* and Xin A. Yang[a]

*The Key Laboratory of Road and Traffic Engineering, Ministry of Education, Tongji University, Shanghai 201804, China*

*(Received December 19, 2020, Revised March 28, 2021, Accepted July 8, 2021)*

**Abstract.** The [BQ] method is a rock mass classification method to evaluate the quality of the rock mass and determine the construction parameters. This method is more empirical and cannot provide predictions for the deformation of tunnels after excavation. To predict the surrounding rock deformation of deep-buried tunnels by using the [BQ] method in China, first, data of 52 tunnels were collected and analyzed to determine the relationship between the grades of the surrounding rock, excavation method, burial depth, tunnel span, and surrounding rock deformation. Second, the equivalence of different surrounding rock grades to the range of geological strength index (GSI) scores were determined using methods, such as fitting GSI to another classification system RMR and RMR to BQ, and considering the correction factors of BQ values. This approach provides the basis for theoretical calculations based on the Hoek–Brown strength criterion. On the basis of the Hoek–Brown strength criterion, a theoretical approach to the deformation of surrounding rock under three failure models, namely, elastic–brittle–plastic, strain-softening, and elastic-perfectly-plastic, is presented when considering the installation time of primary support and the volumetric force of bolts. Finally, the theoretical approach is analyzed and compared with the measured data to verify its feasibility. Moreover, the effects of burial depth, grades of surrounding rock, support parameters, support time, and deformation allowance of the surrounding rock are analyzed. Analysis results can provide some guidance for the prediction of surrounding rock deformation of deep-buried tunnels in China.

**Keywords:** [BQ] method; deep-buried tunnels; deformation; failure model; Hoek-Brown strength criterion

## 1. Introduction

Deformation of surrounding rock has been a core research area in tunnel engineering (Graziani *et al*. 2005, Park 2017, Ranjbarnia *et al*. 2020). Although deformation of surrounding rock is a mandatory measurement in tunnel construction, local collapses caused by inadequate support design are common. At present, the study of surrounding rock deformation mainly includes monitoring, measurement, numerical simulation, and theoretical calculation; these approaches have played important roles in engineering practice. Numerical simulation and field monitoring analysis are common tools to ensure tunnel construction safety (Bizjak and Petkovsek 2004, Barla *et al*. 2010, Satici and Unver 2015, Kong *et al*. 2020, Yertutanol *et al*. 2020). However, numerical simulation and on-site monitoring are used for specific projects. Thus, providing reference for other tunnels to be built is difficult. Theoretical methods are easier to summarize than other methods and usually apply elastoplastic theory to deep-buried tunnels. Thus, the object of this study includes deep-buried tunnels. With regard to the theoretical results on the deformation of tunnel surrounding rock, some scholars provided analytical solutions for radial displacement of deep-buried chambers (Carranza-Torres and Fairhurst 1999, Park and Kim 2006, Wu *et al*. 2021a, 2021b, 2021c, Zhou *et al*. 2021). Moreover, the interaction between the surrounding rock and support structure on this basis was considered (Oreste 2003, Cui *et al*. 2019, Wu and Shao 2019, Wu *et al*. 2020a, 2020b). However, at this stage, the theoretical results require detailed parameters of surrounding rock to predict the deformation that they produced. This task consumes considerable human and material resources. Therefore, summarizing the overall deformation pattern of the tunnel is urgently required.

To control the deformation of the surrounding rock, the Chinese tunnel specifications generally classify the different tunnel sections into different grades to determine the support design. The classification advantage of the surrounding rock grades is that the discontinous fissures, surrounding geological environment, and other conditions, which can be used to estimate the support design, are considered. At present, with the vigorous development of highway and railway construction in China, a large number of mountain tunnels have been built and a wealth of measured data has been accumulated. Thus, the foundation for the study of the different surrounding rock grades in accordance with the overall deformation behavior in tunnel sections has been laid. Fang *et al*. (2014) compiled data on the convergence of surrounding rock deformation in some mountain tunnels in China and obtained the relationships between deformation and factors, such as surrounding rock grade and tunnel excavation size. However, the obtained deformation characteristics of the surrounding rock do not

*Corresponding author, Ph.D. Student
E-mail: 1982426967@qq.com
[a]Ph.D. Student



ISSN: 2005-307X (Print), 2092-6219 (Online)

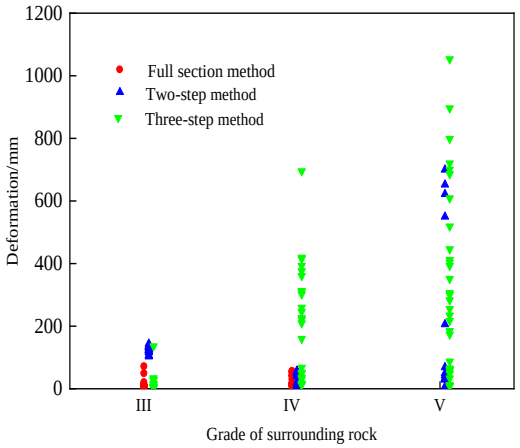


Fig. 1 Deformation monitoring values of tunnel for different surrounding rock grades

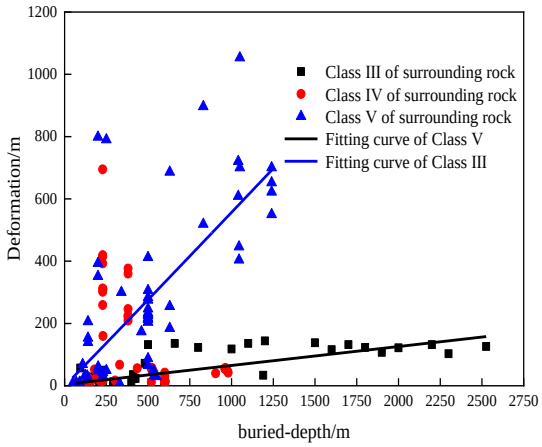


Fig. 2 The relationship between buried-depth and deformation of tunnels

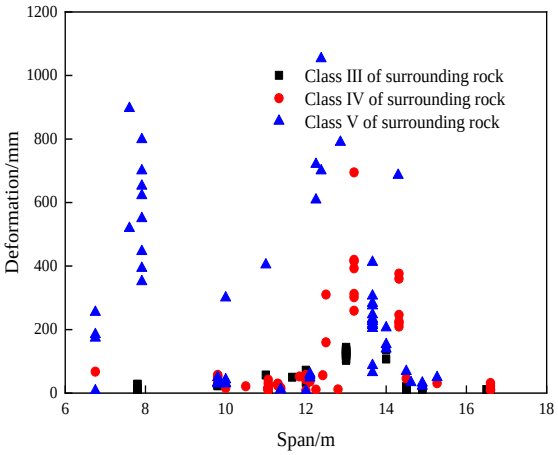


Fig. 3 Relationship between tunnel section span and deformation

provide predictions for other tunnel deformation. Therefore, providing a prediction method for deformation of surrounding rock in conjunction with theoretical calculations is necessary.

Moreover, many factors affect the deformation of surrounding rock, mainly including the grades of surrounding rock, burial depth, section size, and other parameters. The parameters, such as burial depth and section size, are often reflected in the theoretical methods. However, surrounding rock grade cannot be directly applied because the theoretical method requires specific surrounding rock parameters. The methods of surrounding rock classification mainly include RMR method, Q-system method, [BQ] method, and GSI method (Bieniawski 1973, Barton *et al*. 1974, Hoek 1994, National Standards Compilation Group of People's Republic of China 2014). RMR, Q-system, and BQ cannot be directly applied to the theoretical calculation, whereas GSI is an important parameter of Hoek–Brown strength criterion. Therefore, other surrounding rock classification methods can be theoretically calculated by converting GSI values. The results of the Hoek–Brown strength criterion application to the theoretical approach to obtain surrounding rock deformation are as follows. Ground reaction curves were obtained by Park *et al*. (2008) using strain incremental method. Osgoui and Oreste (2010) provided a solution for the surrounding rock deformation under bolts action by using the Hoek–Brown strength criterion. Cui *et al*. (2020) solved the surrounding rock deformation under the elastic–brittle–plastic, strain–softening, and elastic–perfectly–plastic models by conducting a two–stage analysis. Therefore, the Hoek–Brown strength criterion is applicable to solve the deformation of tunnel sections with different grades of the surrounding rock.

This study aims to statistically calculate the surrounding rock deformation changes of typical deep-buried tunnels in part of China and provide deformation solutions by using Hoek–Brown strength criterion for elastic–brittle–plastic, strain-softening, and elastic-perfectly-plastic models. The study is expected to provide some guidance for the deformation prediction of deep-buried tunnels in Chinese mountains by using the [BQ] method to classify surrounding rock grades.

## 2. Monitoring deformation analysis of deep-buried tunnel

In this study, the deformation of deep-buried tunnels in China based on the [BQ] method for classifying the grades of surrounding rock with 178 sections in 37 tunnels will be discussed, as shown in Table 1. The main construction methods of deep-buried tunnels include full-section method, two-step method and three-step method, and the excavation method for part of the Class III and IV surrounding rock sections is full-section method, and the three-step method is mainly distributed in Class IV and V surrounding rock.

Fig. 1 shows the measured deformation values of the tunnels in different grades of the surrounding rock. The maximum value of the monitored deformation is 144 mm for Class III, 419.3 mm for Class IV, and 1000 mm for Class V. The full section method not only accelerates the construction progress, but also reduces the deformation of the surrounding rock, which is suitable for tunnel sections

Table 1 Statistical samples of tunnel deformations

| Tunnel name | Grades of surrounding rock | Number of sections | Buried depth /m | Span /m | Construction Method |
|---|---|---|---|---|---|
| Jinpin Tunnel | III | 14 | 500 ~ 2525 | 13 | Two-step method |
| Yaojia Tunnel | IV, V | 6 | 123 ~ 630 | 14.62, 6.75 | Three-step method |
| A Highway Tunnel | III | 11 | 148.6 | 7.8 | Three-step method |
| Fengxiangya Tunnel | III | 1 | 94 | 11 | Two-step method |
| Gonghe Tunnel | III | 2 | 660, 700 | 14 | Three-step method |
| Caishenliang Tunnel | IV, V | 5 | 70 ~ 303 | 11.37 | Three-step method |
| Alatan Tunnel | IV, V | 2 | 66.19, 47.09 | 12 | Two-step method |
| Zhegushan Tunnel | III, IV, V | 14 | 410 ~ 980 | 9.8 | Two-step method |
| Zoumaling Tunnel | IV | 1 | 200 | 10.5 | Two-step method |
| A tunnel in the southwest of China | IV, V | 4 | 230 | 10 | Two-step method |
| Xiwan Tunnel | IV, V | 2 | 108, 189 | 14.5 | Two-step method |
| Xinlian Tunnel | V | 7 | 228 | 13.2 | Three-step method |
| Guanjiao Tunnel | V | 1 | 340 | 10 | Three-step method |
| Leigongshan Tunnel | IV | 1 | 179 | 11.84 | Two-step method |
| Luopin Tunnel | IV | 1 | 435 | 12.42 | Two-step method |
| Maoyushan Tunnel | V | 1 | 630 | 14.3 | Three-step method |
| Miaoling Tunnel | IV, V | 6 | 201 | 12.1 | Two-step method |
| Zhongtiaoshan Tunnel | IV | 1 | 175 | 12.8 | Two-step method |
| Xishan Tunnel | III | 1 | 225.6 | 11.66 | Full section method |
| Jiahuoyan Tunnel | IV | 4 | 520 ~ 535 | 12 | Full section method |
| Mayazi Tunnel | IV | 4 | 213 | 11.3 | Two-step method |
| Fuchuan Tunnel | V | 3 | 200 | 15.12 | Three-step method |
| Wofoshan Tunnel | V | 2 | 1045 | 11 | Three-step method |
| Wushaoling Tunnel | V | 2 | 1050 | 12.38 | Three-step method |
| A tunnel in the Qinling Mountains | III | 1 | 400 | 16.5 | Two-step method |
| Zhongyi Tunnel | V | 4 | 1240 | 7.91 | Two-step method |
| Badong Water-induced Tunnel | III | 1 | 1190 | 12 | Three-step method |
| Wuduxi Tunnel | V | 2 | 1040 | 12.25 | Three-step method |
| Guanshan Tunnel | V | 2 | 831 | 7.6 | Three-step method |
| Yanmenguan Tunnel | V | 13 | 500 | 13.66 | Three-step method |
| Dabanshan Tunnel | III | 1 | 480 | 12 | Full section method |
| Hulushan Tunnel | III, V | 6 | 135 | 14.9 | Three-step method |
| Erlanshan Tunnel | III, IV | 27 | 600 | 11.06 | Full section method |
| Anfeng Tunnel | III | 6 | 134 ~369 | 14.5 | Two-step method |
| Yuliao Tunnel | III | 7 | 103 ~143 | 16.6 | Full section method |
| Gupanshan Tunnel | III, IV | 8 | 115 ~ 291 | 16.6 | Two-step method |
| Dailing Tunnel | III | 4 | 67 ~ 90 | 14.5 | Full section method |

with good surrounding rock conditions. When the surrounding rock conditions are very poor, the three-step method, which is a step-by-step excavation, still cannot effectively control the deformation of the surrounding rock. Thus, the construction scale should be adjusted, ultra-short step excavation should be performed, and the primary support stiffness should be increased. Moreover, the two-step method of excavation is not recommended for the surrounding rock.

Fig. 2 shows that the deformation of the surrounding rock tends to increase with the increase in burial depth. The deformation of Classes III and V shows a linear change with burial depth, and the deformation of Class IV has no evident correlation with burial depth. The deformation of Classes III, IV, and V is generally controlled within 150, 400, and 800 mm, respectively. Fig. 3 shows the relationships between surrounding rock deformation and tunnel section span, and no significant correlation is found between span and deformation.

Since the criteria for surrounding rock classification in China is different from those in the Europe and the United States, the scores for classification grades based on the [BQ] method in China can be equivalent to the GSI scores, and the prediction of deformation for different surrounding rock grades can be given based on the Hoek–Brown strength criterion.

## 3. Equivalent analysis between [BQ] and GSI

[BQ] considers three coefficients as groundwater conditions $k_1$, orientation of weakness zone related to the

excavation $k_2$ and in situ stress conditions $k_3$. [BQ] can generally be expressed by

$$[\mathrm{BQ}] = \mathrm{BQ} - 100(k_1 + k_2 + k_3) \tag{1}$$

where BQ stands for basic quality system.

Different surrounding rock grades in the [BQ] system correspond to different [BQ] scores, such as [BQ]>550 in Class I, [BQ]=550–450 in Class II, [BQ]=450–350 in Class III, [BQ]=350–250 in Class IV and [BQ]<250 in Class V.

The relationship between [BQ] and GSI scores has not been summarized yet, but some scholars have summarized the RMR system for surrounding rock classification in European areas which the relationship between RMR and [BQ] or GSI. According to the RMR system proposed by Bieniawski (1976), the following relationship exists between GSI and RMR.

$$\mathrm{GSI} = \mathrm{RMR} \tag{2}$$

Xu *et al.* (2014) studied the relationship between BQ and RMR according to the equivalent principle of friction angle and deformation modulus in rock mass, with the following equation as follows.

$$\mathrm{BQ}=170\ln\frac{15+0.24\mathrm{RMR}}{5.7-0.06\mathrm{RMR}} \tag{3}$$

The calculation of [BQ] is given by the Standard for Engineering Classification of Rock Masses (2014), and combined with Eqs. (2) and (3), [BQ] can be expressed as

$$[\mathrm{BQ}]=170\ln\frac{15+0.24\mathrm{GSI}}{5.7-0.06\mathrm{GSI}}-100(k_1+k_2+k_3) \tag{4}$$

With regard to the values of $k_1$, $k_2$ and $k_3$, the Standard for Engineering Classification of Rock Masses gives a range according to different conditions. $k_1$ and $k_2$ can take the mean value. According to the above-mentioned monitoring tunnel deformation, high in-situ stresses are dominated by soft rock tunnels. When the grade of surrounding rock is in Class IV or above grade, $k_3$ can take a value of 0.5 and other surrounding rock grades get a value of 0. Then the coefficient factors are as shown in Table 2.

Substituting the [BQ] ranges for different surrounding rock grades into Eqs. (3) and (4) yields the GSI ranges for different surrounding rock grades, as shown in Table 3.

Hoek and Brown (1997) found that the post-peak mechanical behavior of rock mass is related to the quality of rock mass through extensive engineering practice. When GSI>75, the rock mass exhibits elastic-brittle-plastic failure characteristic. When 25<GSI<75, the rock mass exhibits strain-softening characteristic. Moreover, When GSI<25, the rock mass exhibits elastic-perfectly-plastic behavior. Combined with Table 3, it is found that based on the [BQ] method, the Class I of surrounding rock undergoes bouncing and brittle destruction, while most of surrounding rock plastic zones in Class II, III and IV exhibit strain-softening. Some Class V sections of surrounding rock exhibit strain-softening and another exhibit elastic–perfectly–plastic behavior. Therefore, the corresponding constitutive structure models for different surrounding rock

Table 2 Recommended values for correction factors

| Grades of surrounding rock | I | II | III | IV | V |
|---|---|---|---|---|---|
| $k_1$ | 0.1 | 0.15 | 0.3 | 0.55 | 0.7 |
| $k_2$ | 0.3 | 0.3 | 0.3 | 0.3 | 0.3 |
| $k_3$ | 0 | 0 | 0 | 0.5 | 0.5 |

Table 3 Correspondence between GSI and [BQ]

| Grades of surrounding rock | I | II | III | IV | V |
|---|---|---|---|---|---|
| [BQ] | >550 | 550-451 | 450-351 | 350-251 | ≤250 |
| GSI | >77 | 77-67 | 66-54 | 53-39 | ≤38 |

Table 4 Correspondence between GSI and [BQ]

| Class of rock | I | II | III | IV | V | V |
|---|---|---|---|---|---|---|
| [BQ] | >550 | 550-451 | 450-351 | 350-251 | 250-168 | ≤167 |
| Constitutive model | Elastic-brittle-plastic | Strain-softening | | | | Elastic-perfectly-plastic |

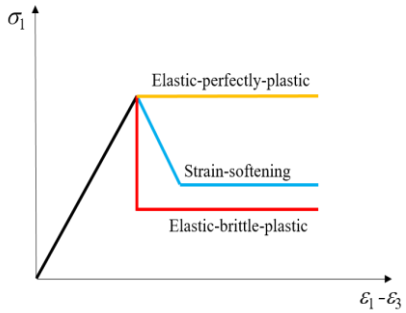


Fig. 4 Three damage models of surrounding rock

grades can be further given, as shown in Table 4. The three damage models are shown in Fig. 4. Therefore, it is necessary to have a theoretical discussion on deformation of surrounding rock to consider the post-peak damage behavior.

## 4. Theoretical analysis

### *4.1 Basic assumptions*

In order to facilitate the derivation of deep-buried tunnels' deformation at different grades of surrounding rock, a number of assumptions are made as follows.

(1) Although the environment in which the rock mass located is complex, the rock mass can be viewed as a homogeneous, continuous rock mass and calculated by using the Hoek-Brown criterion after equating the field rock mass to the GSI. The mechanical behavior of surrounding rock can be described in terms of elastoplasticity.

(2) A tunnel with a circular cross-section and its radius is $r_0$ .Tunnel is subject to hydrostatic pressure at infinity.

(3) The in-situ stress $p_o$ of tunnel is generally considered to relate to the weight $\gamma$ of rock mass and burial depth $H$ of tunnel. The linkage formula is $p_o = \gamma H$.

(4) Since the secondary lining is installed with the tunnel deformation basic stability, then only the suppression of surrounding rock deformation by primary support is considered.

### *4.2 Basic guidelines*

The Hoek–Brown strength criterion has been continually revised to form the generalized Hoek–Brown strength criterion, as follows (Hoek 2002)

$$\sigma_\theta = \sigma_r + \sigma_{\mathrm{ci}}\left(m_{\mathrm{b}}\frac{\sigma_r}{\sigma_{\mathrm{ci}}} + s\right)^a \tag{5}$$

where, $m_b$, $S$ and $a$ can be characterized by geological strength index (GSI) as

$$m_{\mathrm{b}} = m_{\mathrm{i}} \exp\left(\frac{\mathrm{GSI}-100}{28-14D}\right) \tag{6}$$

$$s = \exp\left(\frac{\mathrm{GSI}-100}{9-3D}\right) \tag{7}$$

$$a = \frac{1}{2} + \frac{1}{6}\left[\exp\left(\frac{-\mathrm{GSI}}{15}\right) - \exp\left(\frac{-20}{3}\right)\right] \tag{8}$$

where $D$ is the factor that depends upon the degree of disturbance by blast damage and stress relaxation, which is regarded as 0 in this analysis.

GSI is a factor that is related to the degree of disturbance caused by blast damage and stress relaxation. Cui *et al*. (2017) had given the reasonable relationship between $m_i$ and GSI by

$$m_{\mathrm{i}} = 0.7375\mathrm{GSI}^{0.7586} \tag{9}$$

### *4.3 Stress release coefficient of excavation face*

The tunnel longitudinal excavation diagram is shown in Fig. 5, the stress release coefficient on surrounding rock affected by excavation surface in the 3D tunnel calculation is taken into account. It can be seen that the radial stress of surrounding rock in tunnel wall is not zero within a certain range of the excavation surface, and the fictitious support pressure is as follows.

$$p_{\mathrm{a}}(X) = \left[1-\chi(X)\right]p_0 \tag{10}$$

where $X$ is the axial distance between the monitored point and the excavation face. $\chi(X)$ is the stress releasing rate.

The stress of surrounding rock will be gradually released during the advancement of excavation face, and the stress release rate of surrounding rock can be expressed as follows (Feng *et al*. 2009).

$$\chi(X) = 1 - \mathrm{e}^{-X/L_{\mathrm{A}}} \tag{11}$$

where $L_A$ is the radius of influence of the excavation face, the recommended value is 0.7.

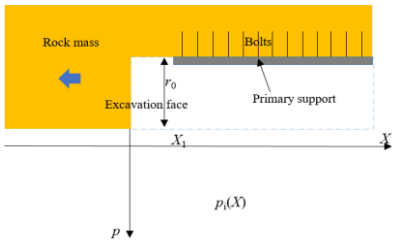


Fig. 5 Longitudinal excavation model of tunnel

### *4.4 Case 1(Elastic-brittle-plastic)*

Combined with the stress release coefficient of three–dimensional excavation of tunnel, the stress and deformation in the non–anchorage–elastic zone after primary support installed can be expressed as

$$\begin{cases} \sigma_r^{\mathrm{e1}} = \chi(X)\,p_0\left[1-\dfrac{L_0^2}{r^2}\right] + \sigma_{r\mathrm{L}_0}\dfrac{L_0^2}{r^2} \\ \sigma_\theta^{\mathrm{e1}} = \chi(X)\,p_0\left[1+\dfrac{L_0^2}{r^2}\right] - \sigma_{r\mathrm{L}_0}\dfrac{L_0^2}{r^2} \\ u^{\mathrm{e1}} = \dfrac{(1+\mu)\left[\chi(X)\,p_0 - \sigma_{r\mathrm{L}_0}\right]}{E}\dfrac{L_0^2}{r} \end{cases} \tag{12}$$

where $\sigma_r^{\mathrm{e1}}$ and $\sigma_\theta^{\mathrm{e1}}$ are the radial stress and tangential stress in the non-anchorage elastic zone, respectively. $E$ and $\mu$ represent the elastic modulus and Poisson's ratio of the surrounding rock, respectively. $\sigma_{r\mathrm{L}_0}$ is the radial stress at the elastoplastic boundary. $L_0$ represents the distance between the distal ends of bolts and the center of the tunnel.

Equilibrium differential equation for considering bolt volume force after bolts installed is as follows.

$$\frac{\mathrm{d}\sigma_r}{\mathrm{d}r} + \frac{\sigma_r - \sigma_\theta}{r} - \frac{dT_r}{s_\theta s_z} = 0 \tag{13}$$

When the strain of bolts after installation is taken into account, $T_r$ can be expressed as

$$T_r = E_{\mathrm{b}} A_{\mathrm{b}} \varepsilon_r \tag{14}$$

According to the generalized Hooke's law, the stress-strain formula of the anchorage elastic zone is as follows.

$$\varepsilon_r = \frac{1-\mu^2}{E}\left(\sigma_r - \frac{\mu}{1-\mu}\sigma_\theta\right) \tag{15}$$

The relationship between stress and deformation of anchorage elastic zone can be modified as

$$\begin{cases} \sigma_r = \dfrac{E(1-\mu)}{(1+\mu)(1-2\mu)}\left(\dfrac{\mathrm{d}u}{\mathrm{d}r} + \dfrac{\mu}{1-\mu}\dfrac{u}{r}\right) \\ \sigma_\theta = \dfrac{E(1-\mu)}{(1+\mu)(1-2\mu)}\left(\dfrac{u}{r} + \dfrac{\mu}{1-\mu}\dfrac{\mathrm{d}u}{\mathrm{d}r}\right) \end{cases} \tag{16}$$

Combining Eqs. (14) and (15) and (16), the result is organized as

$$A_1\frac{\mathrm{d}^2u}{\mathrm{d}r^2}+\frac{A_2}{r}\frac{\mathrm{d}u}{\mathrm{d}r}+\frac{A_2}{r^2}u=0 \tag{17}$$

where $A_1$ and $A_2$ are given by

$$A_1=\frac{E(1-\mu)}{(1+\mu)(1-2\mu)}\left(1-\frac{E_bA_b}{s_\theta s_z}\frac{1-\mu^2}{E}\right)+\frac{E_bA_b}{s_\theta s_z}\frac{\mu^2}{E}\frac{E}{(1-2\mu)} \tag{18}$$

$$\begin{aligned}A_2=&\frac{E\mu}{(1+\mu)(1-2\mu)}\left(1-\frac{E_bA_b}{s_\theta s_z}\frac{1-\mu^2}{E}\right)\\&+\frac{E_bA_b}{s_\theta s_z}\frac{\mu}{E}\frac{E(1-\mu)}{(1-2\mu)}+\frac{E}{(1+\mu)}\end{aligned} \tag{19}$$

Since the deformation at boundary condition $r=R_p$ is equal, the displacement of the non-anchorage-elastic zone can be expressed as

$$\begin{aligned}u^{e2}=&\frac{(\frac{A_1}{A_2}+1)L_0u^{e1}\big|_{r=L_0}-\left[\frac{2\mu-1}{(1-\mu)L_0}u^{e1}\big|_{r=L_0}-p_a(X)\right]L_0^{\frac{A_1}{A_2}+2}}{(\frac{A_1}{A_2}+1)r}\\&+\frac{\left[\frac{2\mu-1}{(1-\mu)L_0}u^{e1}\big|_{r=L_0}-p_a(X)\right]L_0^{\frac{A_1}{A_2}+3}}{(\frac{A_1}{A_2}+1)r^{\frac{A_1}{A_2}+2}}\end{aligned} \tag{20}$$

The anchorage-plastic zone has a compatible equation expressed as

$$\frac{\mathrm{d}\varepsilon_\theta^{p1}}{\mathrm{d}r}+\frac{\varepsilon_\theta^{p1}-\varepsilon_r^{p1}}{r}=0 \tag{21}$$

The anchorage-plastic zone is divided into $m$ rings and where the boundary conditions elastoplastic junction and tunnel wall are the 0th and $m$th rings, respectively. Then the plastic strain relationship between the $j$th ring and the $j$-1th ring is

$$\begin{cases}\varepsilon_{\theta(j)}^{p1}=\varepsilon_{\theta(j-1)}^{p1}+\Delta\varepsilon_{\theta(j)}^{p1}\\ \varepsilon_{r(j)}^{p1}=\varepsilon_{r(j-1)}^{p1}+\Delta\varepsilon_{r(j)}^{p1}\end{cases} \tag{22}$$

Eq. (21) can be rewritten as

$$\frac{\varepsilon_{\theta(j)}^{p1}-\varepsilon_{\theta(j-1)}^{p1}}{r_j-r_{j-1}}+\frac{\varepsilon_{\theta(j)}^{p1}-\varepsilon_{r(j)}^{p1}}{(r_j+r_{j-1})/2}=0 \tag{23}$$

The effect of rock expansion after brittle destruction of surrounding rock is taken in account. Then the equation is

$$\Delta\varepsilon_{r(j)}^{p1}+\alpha\Delta\varepsilon_{\theta(j)}^{p1}=0 \tag{24}$$

For analysis of Former's test data (Former 1988), $\alpha$ generally gets a value from 1.30 to 1.50. So, $a$ can be preferably taken a value of 1.4.

According to Eqs. (22), (23) and (24), the incremental plastic tangential strain of the anchorage-plastic zone can be obtained as follows.

$$\Delta\varepsilon_{\theta(j)}^{p1}=\frac{\left(\varepsilon_{r(j-1)}^{p1}-\varepsilon_{\theta(j-1)}^{p1}\right)\frac{r_j-r_{j-1}}{(r_j+r_{j-1})/2}}{1+2(1+\alpha)\frac{r_j-r_{j-1}}{r_j+r_{j-1}}} \tag{25}$$

The tangential strain of elastoplastic junction is equal and there is

$$\varepsilon_{\theta(0)}^{p1}=\frac{u^{e2}\big|_{r=R_p}}{r} \tag{26}$$

Then the deformation of plastic zone is

$$u_j^{p1}=\left[\varepsilon_{\theta(j-1)}^{p1}+\Delta\varepsilon_{\theta(j)}^{p1}\right]r_j \tag{27}$$

In order to get the deformation of tunnel wall, the radial stress in the anchorage-plastic zone is obtained firstly. According to the combination of Eqs. (5), (13) and (14), the differential equation of equilibrium can be expressed as follows.

$$\begin{aligned}&\frac{\sigma_{r\,(j-1)}^{p1}-\sigma_{r\,(j)}^{p1}}{r_{j-1}-r_j}-\frac{E_bA_b}{s_\theta s_z}\varepsilon_{r(j)}\\&-\frac{2\sigma_{ci}\left(m_b^r\frac{\sigma_{r\,(j-1)}^{p1}+\sigma_{r\,(j)}^{p1}}{2\sigma_{ci}}+s^r\right)^{a^r}}{r_{j-1}+r_j}=0\end{aligned} \tag{28}$$

Rectifying Eq. (28), the relationship between $r_j$ and $r_{j-1}$ can be obtained as

$$\begin{aligned}&\frac{E_bA_b}{s_\theta s_z}\varepsilon_{r(j)}\left(\frac{r_j}{r_{j-1}}\right)^2+\left(2H^r-\Delta\sigma_r\right)\frac{r_j}{r_{j-1}}-\\&\left\{\frac{E_bA_b}{s_\theta s_z}\varepsilon_{r(j)}+\left(2H^r+\Delta\sigma_r\right)\right\}=0\end{aligned} \tag{29}$$

where $H^r=\sigma_{ci}\left(m_b^r\frac{\sigma_{r\,(j-1)}^{p1}+\sigma_{r\,(j)}^{p1}}{2\sigma_{ci}}+s^r\right)^{a^r}$ and $\Delta\sigma_r=\sigma_{r(j)}-\sigma_{r(j-1)}$.

The Eq. (29) is a quadratic equation with $r_j/r_{j-1}$ as the unknown variable. According to the root formula, $r_j/r_{j-1}$ can be found as

$$\frac{r_j}{r_{j-1}}=\frac{-\left[2H^r-\Delta\sigma_r\right]+\sqrt{\left[2H^r-\Delta\sigma_r\right]^2-4\frac{E_bA_b}{s_\theta s_z}\varepsilon_{r(j)}}}{\left\{\frac{E_bA_b}{s_\theta s_z}\varepsilon_{r(j)}+\left[2H^r+\Delta\sigma_r\right]\right\}}\Bigg/\frac{E_bA_b}{s_\theta s_z}\varepsilon_{r(j)} \tag{30}$$

The radius of the plastic zone $R_p$ can be found by Eq. (30). ased on boundary conditions

$$\sigma_{r\,(0)}^{p1}=\sigma_r^{e2}\big|_{r=R_p},\quad \sigma_{r\,(m)}^{p1}=p_i(X) \tag{31}$$

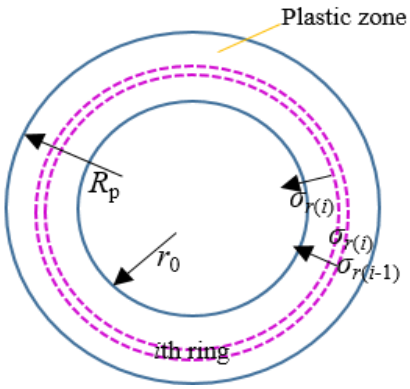


Fig. 6 Schematic diagram of the plastic zone micrometeors

$P_i(X)$ is related to the support stiffness and deformation, then $P_i(X)$ can be given by

$$p_i(X)=K_{all}u_j^{p1}\big|_{j=m} \tag{32}$$

In upright Eqs. (30), (31), (32), tunnel wall deformation $u_m^{p1}$ and the plastic zone radius $R_P$ can be obtained.

If no primary support installed, i.e., when $P_i(X)$=0, the deformation at infinity from the excavation surface can be obtained which can be recorded as $u(\infty)$.

The empirical formula for deformation release factor given by Carranza-Torres and Fairhurst (2000) is

$$\lambda(X)=\left[1+\exp\left(-\frac{X}{1.10}\right)\right]^{-1.7} \tag{33}$$

If the distance from the excavation surface is $X_1$, the deformation of the surrounding rock before the primary support installed can be given by

$$u_1=\lambda(X_1)u(\infty) \tag{34}$$

Then, the total deformation is

$$u_{all}=u_1+u_m^{p1} \tag{35}$$

### *4.5 Case 2 (strain-softening)*

The plastic zone is still generated in surrounding rock after the primary support installed, and the deformation of non-anchorage-elastic zone and anchorage-elastic zone are calculated according to Eqs. (12) and (20).

The anchorage-plastic zone is divided into $n$ concentric micro-element rings, as shown in Fig. 6. It is assumed that the radial stress $\sigma_r$ decreases uniformly along each ring, from the elastoplastic interface $r$=$R_P$ to the distal ends of the bolts $r$=$R_o$. The increment of radial stress named $\Delta\sigma_r$ can be expressed as

$$\Delta\sigma_r=\sigma_{r(i)}-\sigma_{r(i-1)} \tag{36}$$

For the $i$th ring strain in plastic zone, the strain relation is as follows

$$\Delta\eta_{(i)}=\Delta\varepsilon_{\theta(i)}^{p2}-\Delta\varepsilon_{r(i)}^{p2} \tag{37}$$

The strength parameters $m_b$, $s$ and $\alpha$ are a piecewise linear function of $\eta$. The expression is

$$\omega(\eta)=\begin{cases}\omega^p-(\omega^p-\omega^r)\dfrac{\eta}{\eta^*} & 0<\eta<\eta^*\\ \omega^r & \eta\geq\eta^*\end{cases} \tag{38}$$

Anchorage-softening zone has compatible equation as follows

$$\frac{\mathrm{d}\varepsilon_\theta^{p2}}{\mathrm{d}r}+\frac{\varepsilon_\theta^{p2}-\varepsilon_r^{p2}}{r}=0 \tag{39}$$

Eq. (39) can be rewritten as

$$\frac{\varepsilon_{\theta(i)}^{p2}-\varepsilon_{\theta(i-1)}^{p2}}{r_i-r_{i-1}}+\frac{\varepsilon_{\theta(i)}^{p2}-\varepsilon_{r(i)}^{p2}}{(r_i+r_{i-1})/2}=0 \tag{40}$$

The plastic strain of the $i$th ring and $i$-1th ring are as follows.

$$\begin{cases}\varepsilon_{\theta(i)}^{p2}=\varepsilon_{\theta(i-1)}^{p2}+\Delta\varepsilon_{\theta(i)}^{p2}\\ \varepsilon_{r(i)}^{p2}=\varepsilon_{r(i-1)}^{p2}+\Delta\varepsilon_{r(i)}^{p2}\end{cases} \tag{41}$$

In upright Eqs. (37), (40) and (41), the increment of the anchorage plastic tangential strain is found to be

$$\Delta\varepsilon_{\theta(i)}^{p2}=\frac{2\left(\varepsilon_{r(i-1)}^{p2}-\varepsilon_{\theta(i-1)}^{p2}-\Delta\eta_{(i)}\right)}{r_i+r_{i-1}}(r_i-r_{i-1}) \tag{42}$$

Combining Eq. (37) with Eq. (42), the solution of $\Delta\varepsilon_{\theta(i)}^{p2}$ can be solved.

The deformation in plastic zone of the anchorage zone is expressed as

$$u_i^{p2}=\left(\varepsilon_{\theta(i-1)}^{p2}+\Delta\varepsilon_{\theta(i)}^{p2}\right)r_i \tag{43}$$

In order to get the deformation of tunnel wall, the radial stress in anchorage-plastic zone is firstly obtained. According to the combination of Eqs. (12) and (14), the differential equation of equilibrium is expressed as follows.

$$\frac{\sigma_{r\ (i-1)}^{p2}-\sigma_{r\ (i)}^{p2}}{r_{i-1}-r_i}-\frac{2\sigma_{ci}\left(m_b\dfrac{\sigma_{r\ (i-1)}^{p2}+\sigma_{r\ (i)}^{p2}}{2\sigma_{ci}}+s\right)^a}{r_{i-1}+r_i}-\frac{E_bA_b}{s_\theta s_z}\varepsilon_{r(i)}^{p2}=0 \tag{44}$$

Similar to Eq. (30), the relationship of $r_i$ and $r_{i-1}$ can be given by

$$\frac{r_i}{r_{i-1}}=\frac{-[2H-\Delta\sigma_r]+\sqrt{[2H-\Delta\sigma_r]^2-4\dfrac{E_bA_b}{s_\theta s_z}\varepsilon_{r(i)}\left\{\dfrac{E_bA_b}{s_\theta s_z}\varepsilon_{r(i)}+[2H+\Delta\sigma_r]\right\}}}{\dfrac{E_bA_b}{s_\theta s_z}\varepsilon_{r(i)}} \tag{45}$$

where $H=\sigma_{ci}\left(m_b\dfrac{\sigma_{r\ (j-1)}^{p2}+\sigma_{r\ (j)}^{p2}}{2\sigma_{ci}}+s\right)^a$

It is assumed that the $f$th ring of surrounding rock enters plastic residual damage, Eq. (45) further gives the relationship between the radius of the plastic zone $R_p$ and

the radius of the residual zone $R_f$.

$$\frac{R_{\mathrm{f}}}{R_{\mathrm{p}}}=\prod_{i=1}^{f}\frac{-\left[2H-\Delta\sigma_r\right]+\sqrt{\left[2H-\Delta\sigma_r\right]^2-4\dfrac{E_{\mathrm{b}}A_{\mathrm{b}}}{s_\theta s_z}\varepsilon_{r(i)}}}{\dfrac{E_{\mathrm{b}}A_{\mathrm{b}}}{s_\theta s_z}\varepsilon_{r(i)}}\left\{\frac{E_{\mathrm{b}}A_{\mathrm{b}}}{s_\theta s_z}\varepsilon_{r(i)}+\left[2H+\Delta\sigma_r\right]\right\} \tag{46}$$

If only softening zone exists and combined of boundary conditions

$$\sigma_{r\ (0)}^{\mathrm{p2}}=\sigma_r^{\mathrm{e2}}\Big|_{r=R_{\mathrm{p}}},\quad \sigma_{r\ (n)}^{\mathrm{p2}}=p_{\mathrm{i}}(X) \tag{47}$$

The radius of the plastic softening zone $R_p$ and the tunnel wall deformation $u_n^{\mathrm{p2}}$ of surrounding rock can be solved.

If a residual zone exists, considering the effect of rock mass expansion, there is

$$\Delta\varepsilon_{r(j)}^{\mathrm{p2}}+\alpha\Delta\varepsilon_{\theta(j)}^{\mathrm{p2}}=0 \tag{48}$$

According to Eqs. (37), (38) and (43), the radial strain increment of the anchorage plastic zone can be obtained as follows.

$$\Delta\varepsilon_{\theta(i)}^{\mathrm{p2}}=\frac{2\left(\varepsilon_{r(i-1)}^{\mathrm{p2}}-\varepsilon_{\theta(i-1)}^{\mathrm{p2}}\right)}{r_i+r_{i-1}}\left(r_i-r_{i-1}\right) \tag{49}$$

The deformation expression of anchorage-residual zone is consistent with Eq. (35).

In order to solve the tunnel wall deformation, the radial stress in anchorage-plastic zone is firstly obtained, and according to the combination of Eqs. (5) and (13), the differential equation of equilibrium can be expressed as

$$\frac{\sigma_{r\ (i-1)}^{\mathrm{p2}}-\sigma_{r\ (i)}^{\mathrm{p2}}}{r_{i-1}-r_i}-\frac{E_bA_{\mathrm{b}}}{s_\theta s_z}\Delta\varepsilon_{\theta(i)}^{\mathrm{p2}}+\frac{2\sigma_{\mathrm{ci}}\left(m_{\mathrm{b}}^{\mathrm{r}}\dfrac{\sigma_{r\ (i-1)}^{\mathrm{p2}}+\sigma_{r\ (i)}^{\mathrm{p2}}}{2\sigma_{\mathrm{ci}}}+s^{\mathrm{r}}\right)^{a^{\mathrm{r}}}}{r_{i-1}+r_i}=0 \tag{50}$$

Calculation of the relationship between $R_f$ and $r_0$ can be done similarly to Eq. (46). It is important to note that the residual region is not softened, then it can be written as

$$\frac{r_0}{R_{\mathrm{f}}}=\prod_{i=f}^{n}\frac{-\left[2H^{\mathrm{r}}-\Delta\sigma_r\right]+\sqrt{\left[2H^{r}-\Delta\sigma_r\right]^2-4\dfrac{E_{\mathrm{b}}A_{\mathrm{b}}}{s_\theta s_z}\varepsilon_{r(i)}}}{\dfrac{E_{\mathrm{b}}A_{\mathrm{b}}}{s_\theta s_z}\varepsilon_{r(i)}}\left\{\frac{E_{\mathrm{b}}A_{\mathrm{b}}}{s_\theta s_z}\varepsilon_{r(i)}+\left[2H^{r}+\Delta\sigma_r\right]\right\} \tag{51}$$

According to the boundary conditions

$$u_{(f)}^{\mathrm{p2}}=u^{\mathrm{p2}}\Big|_{r=R_{\mathrm{f}}},\quad \sigma_{r\ (n)}^{\mathrm{p2}}=p_{\mathrm{i}}(X) \tag{52}$$

The softening zone radius $R_p$ the residual zone radius $R_f$ and the tunnel deformation $u_n^{\mathrm{p2}}$ can be determined.

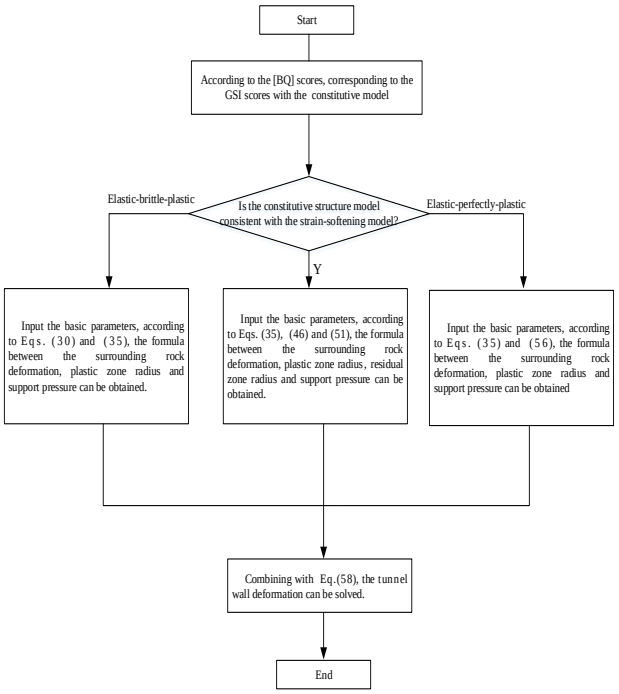


Fig. 7 Flow chart of theoretical calculation

The total deformation is calculated similarly to Case 1 with reference to Eqs. (34) and (35).

### *4.6 Case 3 (elastic-perfectly-plastic)*

The plastic zone of surrounding rock manifests as the elastic-perfectly-plastic failure. The deformation in elastic and anchorage-elastic zones are consistent with Eqs. (12) and (20), respectively. While no volume strain occurs in the plastic zone, the deformation of tunnel wall after primary support installed can be expressed as follows.

$$u^{\mathrm{e2}}(X,L_0)=\frac{R_{\mathrm{p}}}{L_0}u^{\mathrm{p3}}(X,R_{\mathrm{p}}) \tag{53}$$

The anchorage-plastic zone is divided into $l$ rings, the elastoplastic junction and tunnel wall are the 0th and $l$th rings, respectively. The deformation calculation process of anchorage-plastic zone is similar to from Eq. (40) to Eq. (43), the final deformation can be expressed as follows.

$$u_k^{\mathrm{p3}}=\left(\varepsilon_{\theta(k-1)}^{\mathrm{p3}}+\Delta\varepsilon_{\theta(k)}^{\mathrm{p3}}\right)r_k \tag{54}$$

To solve tunnel deformation and according to the combination of Eqs. (5) and (13), the differential equation of equilibrium have the following differential expression.

$$\frac{\sigma_{r\ (k-1)}^{\mathrm{p3}}-\sigma_{r\ (k)}^{\mathrm{p3}}}{r_{k-1}-r_k}-\frac{E_bA_{\mathrm{b}}}{s_\theta s_z}\varepsilon_{r(k)}^{\mathrm{p3}}-\frac{2\sigma_{\mathrm{ci}}^{\mathrm{r}}\left(m_{\mathrm{b}}^{\mathrm{r}}\dfrac{\sigma_{r\ (j-1)}^{\mathrm{p3}}+\sigma_{r\ (j)}^{\mathrm{p3}}}{2\sigma_{\mathrm{ci}}^{\mathrm{r}}}+s^{\mathrm{r}}\right)^{a^{\mathrm{r}}}}{r_{k-1}+r_k}=0 \tag{55}$$

Similar to Eq. (46), the ratio relationship between $R_p$ and

Table 5 Parameters determined by GSI

| GSI | $\sigma_{ci}$ /MPa | $E$ /GPa | $m_b$ | $s$ ($10^{-3}$) | $a$ | $\sigma_{ci}^r$ /MPa | $E^r$ /GPa | $m_b^r$ | $s^r$ ($10^{-3}$) | $a^r$ |
|---|---|---|---|---|---|---|---|---|---|---|
| 90 | 187.02 | 462.14 | 15.67 | 329.19 | 0.500 | 53.74 | 3.46 | 0.92 | 0.55 | 0.519 |
| 85 | 176.98 | 302.13 | 12.55 | 188.87 | 0.500 | 50.08 | 2.96 | 0.83 | 0.45 | 0.521 |
| 80 | 166.59 | 197.53 | 10.03 | 108.37 | 0.501 | 46.57 | 2.54 | 0.74 | 0.37 | 0.524 |
| 75 | 155.76 | 129.14 | 7.99 | 62.18 | 0.501 | 43.21 | 2.18 | 0.66 | 0.30 | 0.527 |
| 70 | 144.46 | 84.43 | 6.34 | 35.67 | 0.501 | 40.02 | 1.87 | 0.59 | 0.25 | 0.531 |
| 65 | 132.68 | 55.19 | 5.01 | 20.47 | 0.502 | 36.99 | 1.61 | 0.52 | 0.20 | 0.535 |
| 60 | 120.46 | 36.09 | 3.95 | 11.74 | 0.503 | 34.12 | 1.38 | 0.46 | 0.17 | 0.539 |
| 55 | 107.92 | 23.59 | 3.09 | 6.74 | 0.504 | 31.42 | 1.18 | 0.41 | 0.14 | 0.544 |
| 50 | 95.26 | 15.42 | 2.41 | 3.87 | 0.506 | 28.88 | 1.02 | 0.35 | 0.11 | 0.550 |
| 45 | 82.74 | 10.08 | 1.86 | 2.22 | 0.508 | 26.50 | 0.87 | 0.31 | 0.09 | 0.556 |
| 40 | 70.65 | 6.59 | 1.42 | 1.27 | 0.511 | 24.28 | 0.75 | 0.26 | 0.07 | 0.564 |
| 35 | 59.28 | 4.31 | 1.07 | 0.73 | 0.516 | 22.21 | 0.64 | 0.22 | 0.06 | 0.572 |
| 30 | 48.89 | 2.81 | 0.80 | 0.42 | 0.522 | 20.3 | 0.55 | 0.19 | 0.05 | 0.581 |
| 25 | 39.67 | 1.84 | 0.58 | 0.24 | 0.531 | 18.52 | 0.47 | 0.15 | 0.04 | 0.591 |
| 20 | 31.71 | 1.20 | 0.41 | 0.14 | 0.544 | 16.88 | 0.41 | 0.12 | 0.03 | 0.603 |

$r_0$ can be given by

$$\frac{r_0}{R_p}=\prod_{k=1}^{l}\frac{-\left[2H-\Delta\sigma_r\right]+\sqrt{\left[2H-\Delta\sigma_r\right]^2-4\dfrac{E_bA_b}{s_\theta s_z}\varepsilon_{r(k)}}\sqrt{\left\{\dfrac{E_bA_b}{s_\theta s_z}\varepsilon_{r(k)}+\left[2H+\Delta\sigma_r\right]\right\}}}{\dfrac{E_bA_b}{s_\theta s_z}\varepsilon_{r(k)}} \tag{56}$$

Based on boundary conditions

$$u_0^{p3}\Big|_{r=R_p}=u^{e2}\Big|_{r=R_p},\quad \sigma_{r(l)}^{p3}=p_i(X) \tag{57}$$

Then the plastic zone radius $R_p$ and the tunnel deformation $u_l^{p3}$ can be determined.

The total deformation is calculated similarly to Case 1 with reference to Eqs. (34) and (35).

### *4.6 Method of support pressure calculation*

The primary support materials are considered to be bolts, shotcrete and steel arches. The contact pressure between the primary support and surrounding rock, taking into account the deformation allowance of the steel arch installation, which is given as $u_0$, is generally expressed as follows.

$$p_i(X)=K_1\Delta u_1(X)+K_s\left[\Delta u_1(X)-u_0\right] \tag{58}$$

The expressions of $K_1$ and $K_2$ are as follows.

$$\begin{cases}K_1=\dfrac{E_1\left(r_0^2-r_1^2\right)}{\left(1+\mu_1\right)\left[\left(1-2\mu_1\right)r_0^2+r_1^2\right]}\\ K_s=\dfrac{E_{st}A_{set}}{S\left(r_0-h_{set}/2\right)^2}\end{cases} \tag{59}$$

Moreover, it should be noted that the values of $m$, $n$, and $l$ should be greater than 100 to ensure the accuracy of the calculation. The specific calculation flow is shown in Fig. 7.

Table 6 Relationship between GSI and $\eta^*$

| GSI | 0 ~25 | 35 | 50 | 60 | 65 | 75 ~100 |
|---|---|---|---|---|---|---|
| $\eta^*$ | $+\infty$ | 0.1 | 0.01 | 0.005 | 0.001 | 0 |

## 5. Theoretical validation and impact factors analysis

### *5.1 Theoretical parameter design*

Section 3 has analyzed the relationship between the range of GSI scores and grades of surrounding rock. To accurately analyze the influence of GSI on the deformation of surrounding rock, it is necessary to clarify the relationship between the GSI scores and the parameters $m_b$, $s$, $\alpha$, $\sigma_{ci}$ and $E$. Relationship between $m_b$, $s$, $\alpha$ and GSI has been given in Eqs. (2), (3) and (4), Hoek and Diederichs (2006), Ajalloeian and Mohammadi (2014) have given suitable relationship between $\sigma_{ci}$, $E$ and GSI, respectively as follows.

$$\sigma_{ci}=\frac{0.5\exp\left(0.06\mathrm{GSI}\right)}{0.0387+0.00474\exp\left(\mathrm{GSI}/18.9086\right)} \tag{60}$$

$$E=0.22\exp(0.085\mathrm{GSI}) \tag{61}$$

Cai *et al*. (2007) obtained the relationship between $\mathrm{GSI}^r$ and GSI in residual zone based on in-situ rock shear tests as

$$\mathrm{GSI}^r=0.36\mathrm{GSI} \tag{62}$$

Then the relationship between the parameters and GSI can be shown in Table 5.

For critical plastic softening coefficient $\eta^*$, the relationship between GSI and $\eta^*$can be given as shown in Table 6 (Cui *et al*.2019).

The value of $\eta^*$ can be determined by fitting.

The radius of the tunnel section is set at $r_0$= 7 m with reference to the monitoring section dimensions. Set the weight of surrounding rock $\gamma$=24 kN/m$^3$, Poisson's ratio $\mu$= 0.25.

Moreover, the support parameters vary slightly

Table 7 Design parameters for composite lining

| Grades of surrounding rock | Primary support | | | | |
|---|---|---|---|---|---|
| | Thickness of shotcrete (C25/cm) | Bolt | | Steel arch | |
| | | Length/m | Inter-row spacing /m | Section steel type | Spacing of steel arch shelf /m |
| I | 6 | / | / | / | / |
| II | 10 | 2.5 | / | / | / |
| III | 15 | 3.0 | 1.2 × 1.2 | / | / |
| IV | 20 | 3.5 | 1.0 × 1.0 | Grille (150) | 1.0 |
| V | 25 | 4.0 | 0.8 × 0.8 | Section steel (I20a) | 0.8 |

Table 8 Basic parameters of support structure

| Support structure | Parameter | Value |
|---|---|---|
| Shotcrete | $E_1$/GPa | 25 |
| | $\mu_1$ | 0.2 |
| | $r_1$/m | 0.15 |
| Bolt | $E_b$/GPa | 206 |
| | $A_b$/cm$^2$ | 12.56 |
| Steel arch | $E_{st}$/GPa | 206 |
| | $A_{set}$/cm$^2$ | 39.578 |
| | $h_{set}$ /mm | 200 |

Table 9 Deformation allowance of surrounding rock

| Grades of surrounding rock | I | II | III | IV | V |
|---|---|---|---|---|---|
| Deformation allowance /mm | / | 30 | 65 | 100 | 125 |

Table 10 Distance from excavation face to primary support

| Grades of surrounding rock | I | II | III | IV | V |
|---|---|---|---|---|---|
| $X_1$/m | 3 | 3 | 1.5 | 0 | 0 |

depending on the rock surrounding grades. With reference to the Design Rules for Road Tunnels, and taking the design parameters of the a three-lane tunnel composite lining as an example. The types of support materials and the support parameters of different surrounding rock grades (average values) are shown in Table 7.

However, Table 7 does not specify the own parameters of the support structure, and the specific parameters of the support structures are given in Table 8 with reference to the material parameters table.

The deformation allowance is taken as the mean value, as shown in Table 9.

There is no specific guidance on support time of primary tunnel installation for different surrounding rock grades. Zhang *et al.* (2017) gave the primary support time through the longitudinal deformation curves of tunnels with different grades of surrounding rock. The distance of Class II, III, and IV of surrounding rock between the excavation face and primary support is +∞, 3.334 m, and 0 m, respectively. Furthermore, the distance between Class I and V surrounding rock and the excavation face is +∞ and 0 m, respectively.

Then recommended support time of primary support installation can be shown in Table 10.

### *5.2 Comparative analysis of theoretical calculations and measurements*

Most GSI scores of the surrounding rock of Classes III and IV conform to the strain-softening model, and the deformation is calculated using the Case 2 theory. The

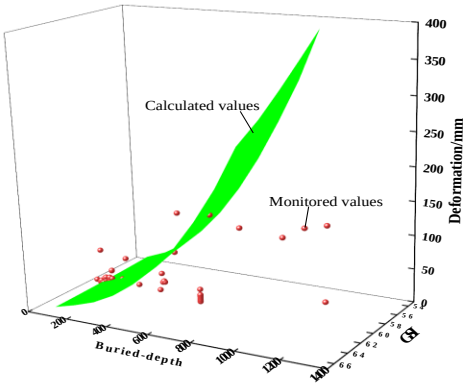


(a) Class III of surrounding rock

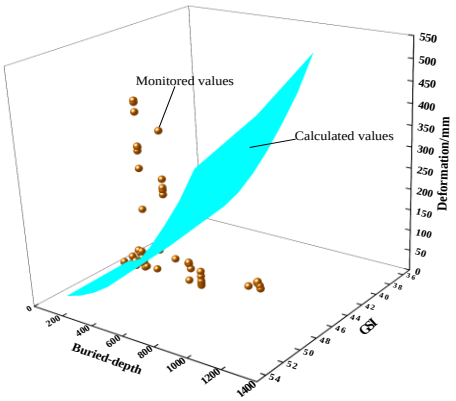


(b) Class IV of surrounding rock

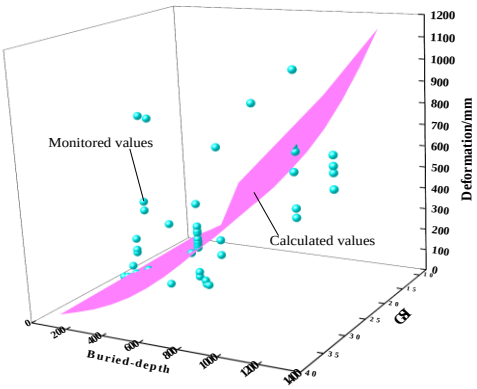


(c)Class V of surrounding rock

Fig. 8 Comparison of theoretical analysis and measured values

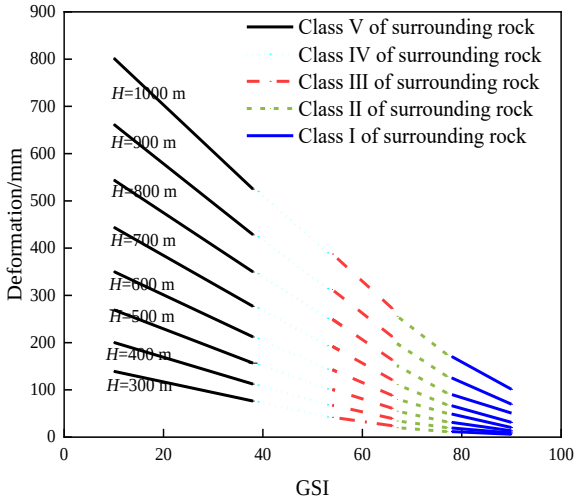


Fig. 9 Effect of burial depth on tunnel deformation for different surrounding rock grades

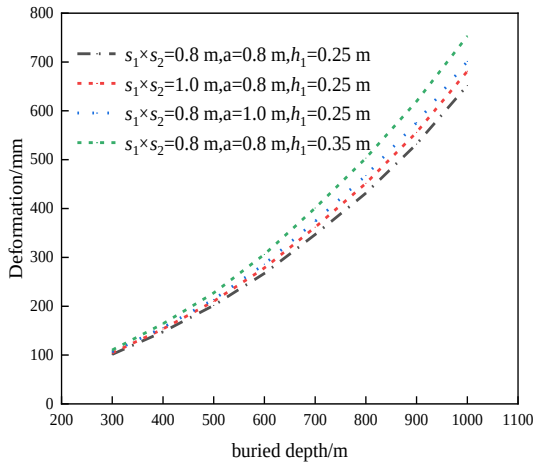


Fig. 10 The effect of support parameters on the surrounding rock deformation of tunnel

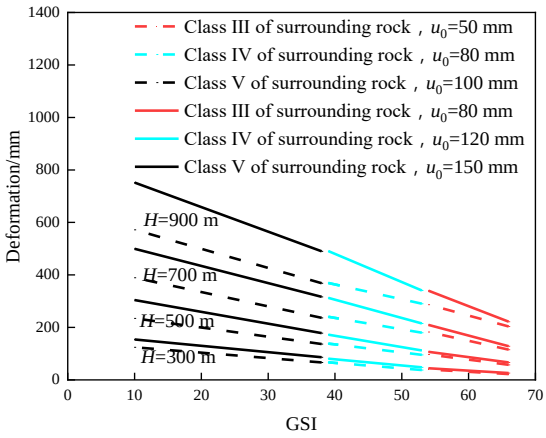


Fig. 11 Effect of deformation allowance on tunnel deformation for different surrounding rock grades

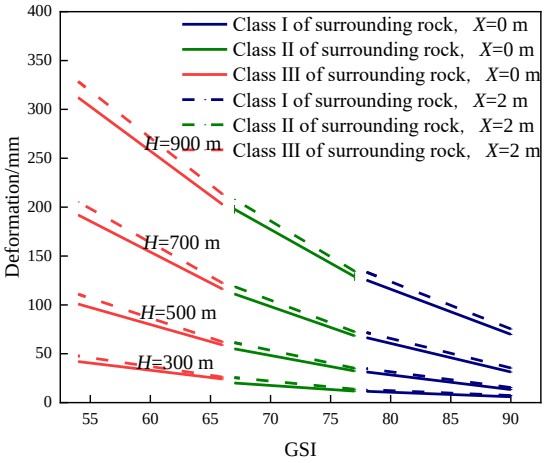


Fig. 12 Effect of primary support time on tunnel deformation for different surrounding rock grades

deformation can be averaged in accordance with the theoretical calculations of Case 2 and Case 3. However, the GSI scores corresponding to the Class V surrounding rock partly conform to the strain-softening model and partly to the elastic-perfectly-plastic model. For example, as shown in Fig. 8, the measured deformation scores of some Class III surrounding rock sections are greater than the theoretical calculation scores when the burial depth is less than 200 m. However, the measured values are generally less than the theoretical calculation values when the burial depth is greater than 200 m. When the burial depth of Class IV surrounding rock is less than 400 m, some sections are destabilized and the deformation is much greater than the theoretical calculation value, while the other measurements are within the theoretical range. The theoretical deformation calculation value of Class V surrounding rock is closer to the average value of the tunnel-monitored deformation. In general, the theoretical calculations are greater than or equal to the measured data, validating the feasibility of Case 2 and Case 3 methods. Case 1 method is applicable to Class I surrounding rock, and published literature about monitored deformation of Class I surrounding rock is limited. Thus, Case 1 calculations are analyzed using the influence of deformation.

### *5.3 Parametric analysis of surrounding rock deformation in deep-buried tunnels*

The deformation errors at the boundaries of the GSI scores of 25 and 75 in the three conditions are disregarded in the lower surrounding rock grade. The deformation values with burial depth for different surrounding grades are shown in Fig. 9. Greater burial depth indicates greater deformation. The larger grade of the surrounding rock indicates greater deformation. Under the same burial depth, the deformation of Class I is smaller than that of Class II. This finding verifies the feasibility of the theoretical method of Case 1. The influence of primary support parameters on the deformation of the surrounding rock is shown in Fig. 10. The distance between bolts, the distance between steel arches, and the thickness of the shotcrete influence the surrounding rock deformation. The thickness of the shotcrete has the greatest influence. Therefore, for the weak surrounding rock, increasing the primary support stiffness

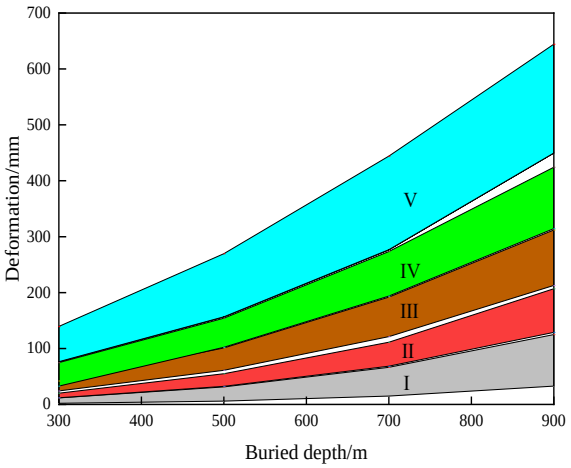


Fig. 13 Range of tunnel deformation with burial depth for different surrounding rock grades

can effectively prevent the surrounding rock destabilization. Fig. 11 shows the influence of the deformation allowance on the surrounding rock deformation. The figure shows that the weaker surrounding rock indicates larger influence of the deformation allowance on the surrounding rock deformation. The deformation allowance of the surrounding rock should be reasonably designed to avoid excessive deformation or excessive force on the primary support. Fig. 12 shows that the smaller distance between primary support and excavation surface indicates smaller deformation of the surrounding rock. However, it has limited effect on suppressing deformation.

### *5.4 Prediction of surrounding rock deformation with different surrounding rock grades*

Fig. 13 shows the variation of the tunnel deformation with depth for different surrounding rock grades. As the depth of the tunnel increases, the deformation of the surrounding rock increases. With a depth of less than 300 m, the deformation of the surrounding rock does not exceed 150 mm. In addition, for a depth of more than 900 m, the deformation of the surrounding rock can exceed 600 mm. The depth of the tunnel with high in-situ stress should be 500 m to limit the deformation of the surrounding rock and ensure the safety of projects.

It is important to note that the results of the study are applicable to deeply buried mountainous tunnels based on the [BQ] method for classification of the surrounding rock grades.

## 6. Conclusions

The factors influencing the tunnel deformation at different surrounding rock grades were demonstrated by systematically analyzing the measured data on the surrounding rock deformation of deep-buried tunnels. The surrounding rock deformation at three cases was analyzed on the basis of the Hoek–Brown strength criterion. The following conclusions were drawn.

• The measured deformation values of Class III and Class IV surrounding rock are generally smaller than the theoretical calculation, and the average measured deformation values of Class V surrounding rock are closer to the theoretical calculation. What can be further predicted is that the measured deformation values of Class I and Class II are smaller than the theoretical calculation. Therefore, the tunnel deformations calculated on the basis of the Hoek–Brown strength criterion are in good agreement with the measurements.

• The deformation of Classes III, IV, and V surrounding rock is generally controlled within 150, 400, and 800 mm, respectively in the measured deformation data. To effectively control the deformation of the surrounding rock, the full-section method can be used to excavate Class III and above, and the three-step method should be used to excavate Class V. For the weak surrounding rock with high in-situ stress, ultrashort step excavation should be used. As the grade or depth of the surrounding rock increases, its deformation increases. This deformation is relatively related to the tunnel span.

• The support parameters influence the deformation of the surrounding rock, and the shotcrete thickness greatly influence the deformation compared with other support parameters. The amount of deformation allowance greatly influences the surrounding rock deformation, whereas the primary support time has limited influence on the surrounding rock deformation. The deformation allowance of weak surrounding rock should be reasonably designed.

• The greater tunnel depth indicates greater deformation variation in different surrounding rock grades. Maximum surrounding rock deformation should be predicted from the tunnel section with greater burial depth on the basis of the surrounding rock grade as a support design reference. It can greatly limit the deformation of the surrounding rock from the viewpoint of improving the support rigidity. The deformation prediction of the different surrounding rock grades can provide some guidance for tunnel construction.

## Acknowledgments

Financial support was received from the National Natural Science Foundation (51178336), Scientific Research Project of Zhejiang Provincial Transportation Department (2017038) for the preparation of this manuscript. This financial support is greatly appreciated.

## References

Ajalloeian, R. and Mohammadi, M. (2014), “Estimation of limestone rock mass deformation modulus using empirical equations”, *Bull. Eng. Geol. Environ.* **73**(2), 541-550. https://doi.org/10.1007/s10064-013-0530-3.

Barton. N., Lien, R. and Lunde, J. (1974), “Engineering classification of rock masses for the design of tunnel support”, *Rock. Mech*. **6**(4), 189-236. https://doi.org/10.1007/BF01239496.

Basarir, H., Genis, M. and Ozarslan, A. (2010), “The analysis of radial displacements occurring near the face of a circular

opening in weak rock mass", *Int. J. Rock. Mech. Min Sci.*, **47**(5), 771-783. https://doi.org/ 10.1016/j.ijrmms.2010.03.010.

Bieniawski, Z.T. (1973), "Engineering classification of jointed rock masses", *Civil Eng. Siviele Ingenieurswese*, **1973**(12), 335-343.

Bieniawski, Z.T. (1976), "Rock mass classification in rock engineering", *Proceedings of the Symposium on Explorer for Rock Engineering*, Johannesburg, 97-106.

Bizjak, K.F. and Petkovsek, B. (2004), "Displacement analysis of tunnel support in soft rock around a shallow highway tunnel at Golovec", *Eng. Geol.*, **75**(1), 89-106. https://doi.org/10.1016/j.enggeo.2004.05.003.

Cai, M., Kaiser, P.K., Tasaka, Y. and Minami, M. (2007), "Determination of residual strength parameters of jointed rock mass using the GSI system", *Int. J. Rock. Mech. Min. Sci.,* **44**(2), 247-265. https://doi.org/ 10.1016/j.ijrmms.2006.07.005.

Carranza-Torres, C. and Fairhurst, C. (1999), "The elasto-plastic response of underground excavations in rock masses that satisfy the Hoek-Brown failure criterion", *Int. J. Rock. Mech. Min. Sci*., **36**(6), 777-809. https://doi.org/ 10.1016/S0148-9062(99)00047-9.

Carranza-Torres, C. and Fairhurst, C. (2000), "Application of the convergence-confinement method of tunnel design to rock masses that satisfy the Hoek-Brown failure criterion", *Tunn. Undergr. Space Tech.* **15**(2), 187-213. https://doi.org/10.1016/S0886-7798(00)00046-8.

Cui, L., Dong, Y.K. and Sheng, Q. (2019), "New numerical procedures for fully-grouted bolt in the rock mass with slip and non-slip cases at the rock-bolt interface", *Construct. Build. Mater.*, **204**, 849-863. https://doi.org/ 10.1016/j.conbuildmat.2019.01.219.

Cui, L., Sheng, Q., Dong, Y.K., Miao, C.X., Huang, J.H. and Zhang, A.J. (2020), "Two-stage analysis of interaction between strain-softening rock mass and liner for circular tunnels", *Eur. J. Environ. Civ. Eng*. 1-26. https://doi.org/10.1080/19648189.2020.1715849.

Cui, L., Sheng, Q., Zheng, J.J., Cui, Z., Wang, A. and Shen, Q. (2019), "Regression model for predicting tunnel strain in strain-softening rock mass for underground openings", *Int. J. Rock. Mech. Min. Sci*. **119**, 81-97.

Cui, L., Zheng, J.J., Dong, Y.K., Pan, Y. and Cui, B. (2017), "Prediction of critical strains and critical support pressures for circular tunnel excavated in strain-softening rock mass", *Eng. Geol.*, **224**(22),43-61. https://doi.org/ 10.1016/j.enggeo.2017.04.022.

Fang, Q., Su, W., Zhang, D.L. and Yu, F.C. (2016), "Tunnel deformation characteristics based on on-site monitoring data", *Chinese. J. Rock. Mech. Eng.*, **35**, 1884-1897. https://doi.org/ 10.13722/j.cnki.jrme.2014.1663.

Feng, X.D., Jimenez, R., Zeng, P. and Senent, S. (2019), "Prediction of time-dependent tunnel convergences using a Bayesian updating approach", *Tunn. Undergr. Space. Tech*., **94**, 103118. https://doi.org/10.1016/j.tust.2019.103118.

Former, I.W. (1988), *Engineering Properties of Rock*, Xuzhou, China University of Mining and Technology Press.

Graziani, A., Boldini, D. and Ribacchi, R. (2005), "Practical estimate of deformations and stress relief factors for deep tunnels supported by shotcrete", *Rock Mech. Rock Eng*., **38**(5), 345-372. https://doi.org/10.1007/s00603-005-0059-2.

Hoek, E. (1994), "Strength of rock and rock masses", *ISRM. News*. J., **2**, 4-16.

Hoek, E. and Brown, E.T. (1997), "Practical estimates of rock mass strength", *Int. J. Rock. Mech. Min. Sci*., **34**(8), 1165-1186. https://doi.org/10.1016/S0148-9062(97)00305-7.

Hoek, E. and Diederichs. M.S. (2006), "Empirical estimation of rock mass modulus", *Int. J. Rock. Mech. Min. Sci*., **43**(2), 203-215. https://doi.org/ 10.1016/j.ijrmms.2005.06.005.

Hoek, E., Carranza-Torres, C. and Corkum, B. (2002), "Hoek-Brown failure criterion-2002 Edition", *In: Proceedings of NARMS-TAC conference*, Toronto, Canada. https://doi.org/ 10.1016/j.ijrmms.2019.04.014.

Kong, X.Y., Chen, X., Tang, C.A., Sun, Z.R. and Hu, E.H. (2020), "Study on large deformation control technology and engineering application of tunnel with high ground stress and weak broken surrounding rock", *Struct. Eng. Int*., 1-9. https://doi.org/10.1080/10168664.2020.1770664.

Oreste, P.P. (2003), "A procedure for determining the reaction curve of shotcrete lining considering transient conditions", *Rock. Mech. Rock. Eng.*, **36**(3),209-236. https://doi.org/ 10.1007/s00603-002-0043-z.

Osgoui, R.R. and Oreste, P.P. (2010), "Elasto-plastic analytical model for the design of grouted bolts in a Hoek-Brown medium", *Int. J. Numer. Anal. Met. Geomech.* **34**(16), 1651-1686. https://doi.org/ 10.1002/nag.823.

Park, K. (2017), "Simple solutions of an opening in elastic-brittle plastic rock mass by total strain and incremental approaches", *Geomech. Eng*., **13**(4), 585-600. https://doi.org/10.12989/gae.2017.13.4.585.

Park, K.H. and Kim, Y.J. (2006), "Analytical solution for a circular opening in an elastic-brittle-plastic rock", *Int. J. Rock. Mech. Min. Sci*., **43**(4), 611-622. https://doi.org/ 10.1016/j.ijrmms.2005.11.004.

Park, K.H., Tontavanich, P. and Lee, J.G. (2008), "A simple procedure for ground response curve of circular tunnel in elastic-strain softening rock masses", *Tunnel. Undergr. Sp. Technol*. **23**(2), 151-159. https://doi.org/ 10.1016/j.tust.2007.03.002.

Ranjbarnia, M., Rahimpour, N. and Oreste, P. (2020), "A new analytical-numerical solution to analyze a circular tunnel using 3D Hoek-Brown failure criterion", *Geomech. Eng*., **22**(1), 11-23. https://doi.org/10.12989/gae.2020.22.1.011.

Satici, O. and Unver, B. (2015), "Assessment of tunnel portal stability at jointed rock mass: A comparative case study", *Comput. Geotech*., **64**, 72-82. https://doi.org/ 10.1016/j.compgeo.2014.11.002.

Wu, K. and Shao. Z.S. (2019), "Study on the effect of flexible layer on support structures of tunnel excavated in viscoelastic rocks", *J. Eng. Mech*., **145**(10), 1-10. https://doi.org/10.1061/(ASCE)EM.1943-7889.0001657.

Wu, K., Shao, Z., Sharifzadeh, M., Hong, S. and Qin, S. (2021), "Analytical computation of support characteristic curve for circumferential yielding lining in tunnel design", *J. Rock Mech. Geotech. Eng*., **13**(1), 1-13.

Wu, K., Shao, Z.S. and Qin, S. (2020a), "An analytical design method for ductile support structures in squeezing tunnels", *Arch. Civ. Mech. Eng*., **20**, 91. https://doi.org/10.1007/s43452-020-00096-0.

Wu, K., Shao, Z.S., Qin, S., Wei, W. and Chu, Z. (2021b), "A critical review on the performance of yielding supports in squeezing tunnels", *Tunn. Undergr. Space. Tech*., 115, 103815. https://doi.org/10.1016/j.tust.2021.103815.

**Wu, K., Shao, Z.S., Qin, S., Zhao, N. and Hong, S. (2021c), "An improved non-linear creep model for rock applied to tunnel displacement prediction", *Int. J. Appl. Mech*., in press.**

Wu, K., Shao, Z.S., Qin, S., Zhao, N. and Hu, H. (2020b), "Analytical-based assessment of effect of highly deformable elements on tunnel lining within viscoelastic rocks", *Int. J. Appl. Mech.*, **12**(3), 2050030. https://doi.org/10.1142/S1758825120500301.

Xu, H.F., Chen, F., Wang, B., Hua, Z.M. and Geng, H.S. (2014), "Relationship between RMR and BQ for rock mass classification and estimation of its mechanical parameters", *Chinese J. Geotech. Eng*. **36** ,195-198. https://doi.org/

10.11779/CJGE201401021.
Yertutanol, K., Haluk, A. and Sopac, E. (2020), "Displacement monitoring, displacement verification and stability assessment of the critical sections of the Konak tunnel, zmir, Turkey", *Tunn. Undergr. Sp. Tech*., **101**,103357. https://doi.org/ 10.1016/j.tust.2020.103357.
Zhang, Y.J., Su, K., Zhou, Li. and Wu, H.G. (2017), "Estimation of ground support installation time based on the tunnel longitudinal displacement of convergence-confinement method", *Rock. Soil. Mech*., **38**(S1), 471-478. https://doi.org/10.16285/j.rsm.2017.S1.058.
Zhou, J., Yang, X.A., Ma, M.J. and Li, L.H. (2021), "The support load analysis of deep-buried composite lining tunnel in rheological rock mass", *Comput. Geotech*. **130**, 103934. https://doi.org/10.1016/j.compgeo.2020.103934.